Supplement of Atmos. Chem. Phys., 25, 8943–8958, 2025
https://doi.org/10.5194/acp-25-8943-2025-supplement

Atmospheric Chemistry and Physics Open Access

Supplement of

Ice crystal complexity leads to weaker ice cloud radiative heating in idealized single-column simulations

Edgardo I. Sepulveda Araya et al.

Correspondence to: Edgardo I. Sepulveda Araya (edgardo@arizona.edu) and Sylvia C. Sullivan (sylvia@arizona.edu)

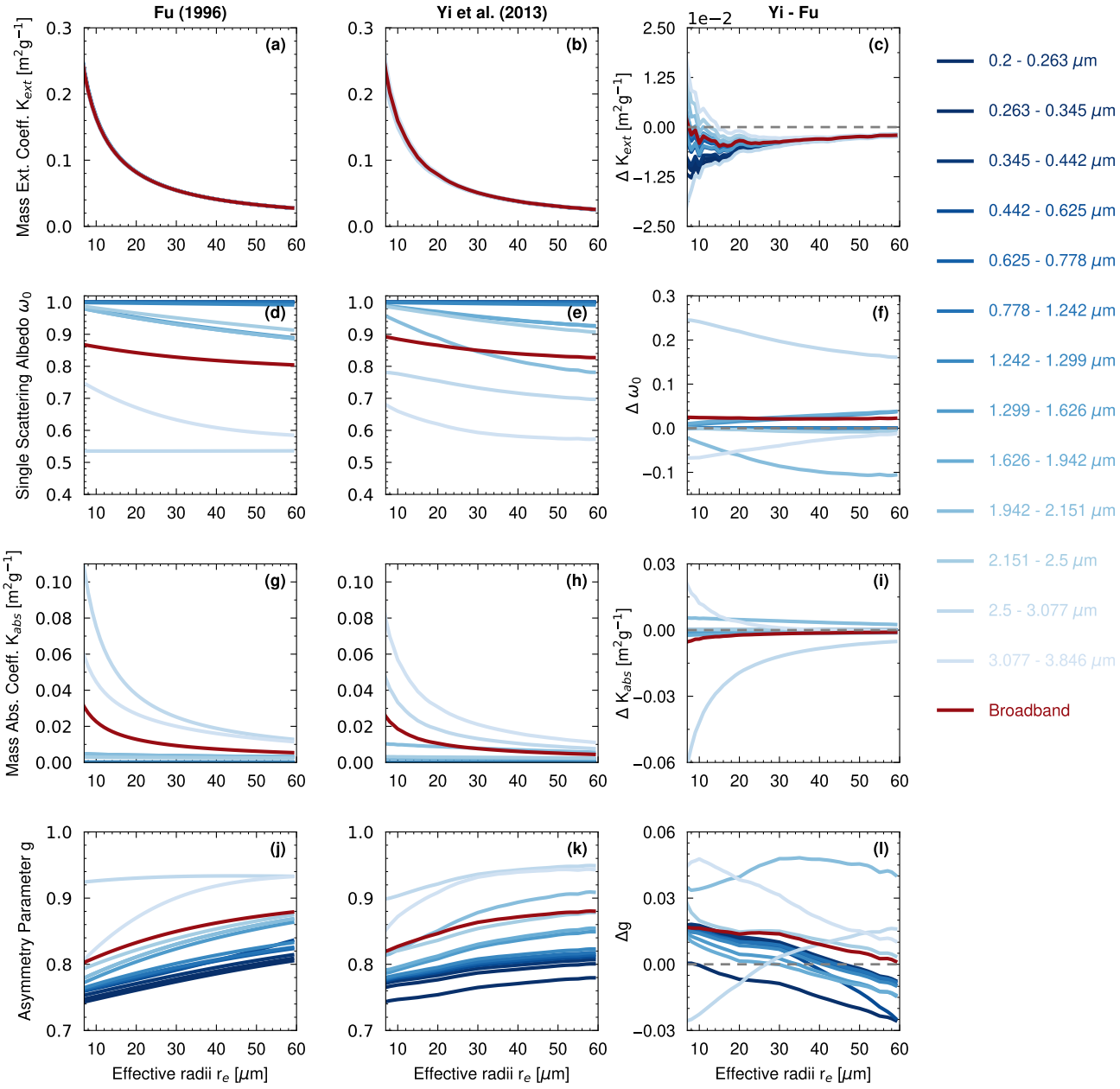

Figure S1. Shortwave (SW) optical parameterizations as a function of ice crystal effective radii. Each row shows the optical properties from top to bottom: mass extinction coefficient K_{ext}, single scattering albedo ω_0, mass absorption coefficient K_{abs} and asymmetry parameter g. The left column shows Fu scheme, the middle column Yi13 scheme, and the interscheme difference is shown in the right column. 13 RRTMG SW bands, and broadband calculation is included in each panel.

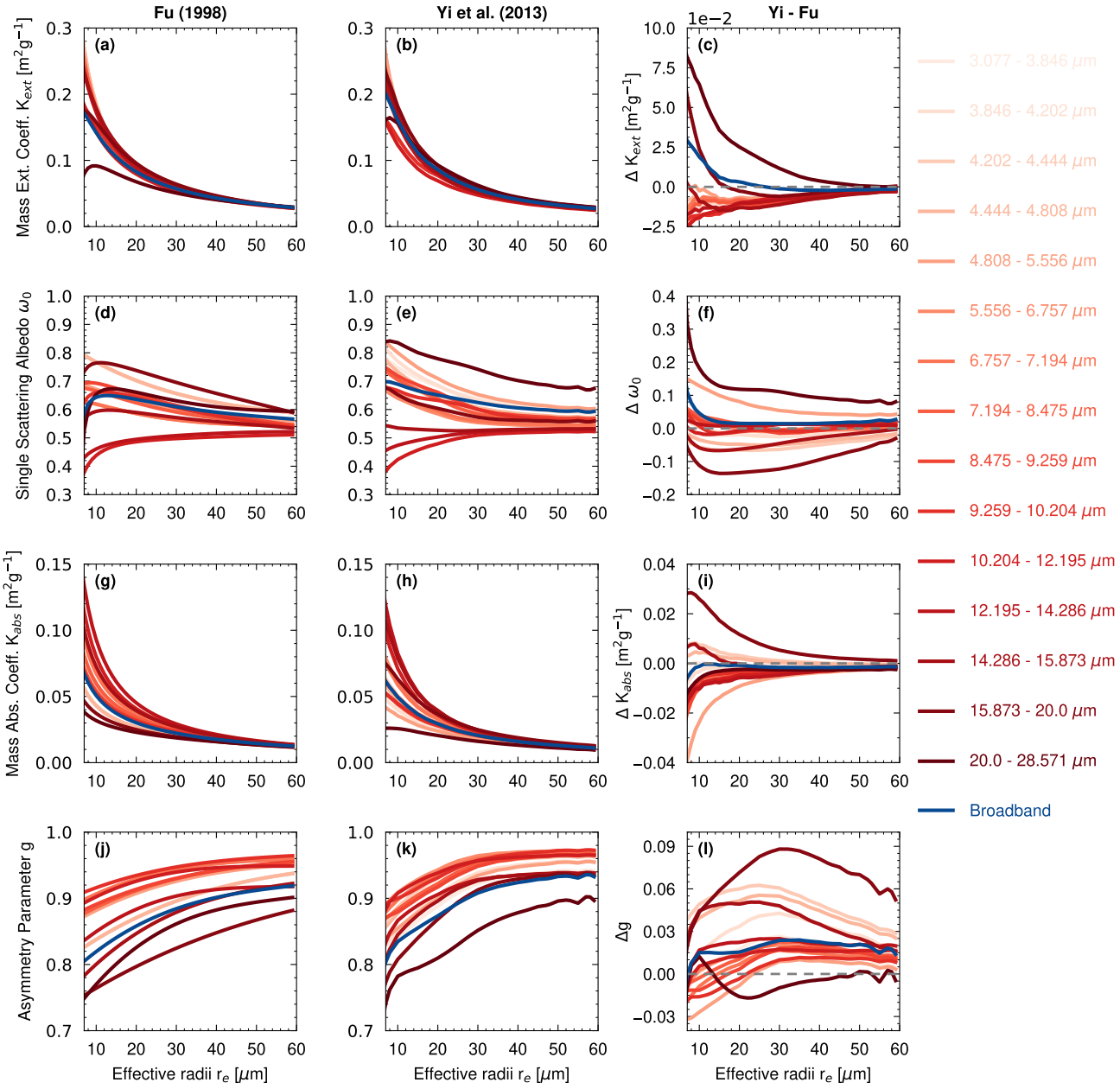

Figure S2. Longwave (LW) optical parameterizations as a function of ice crystal effective radii. Panels distribution are as in Fig. S1. 15 RRTMG LW bands, and broadband calculation is included in each panel.

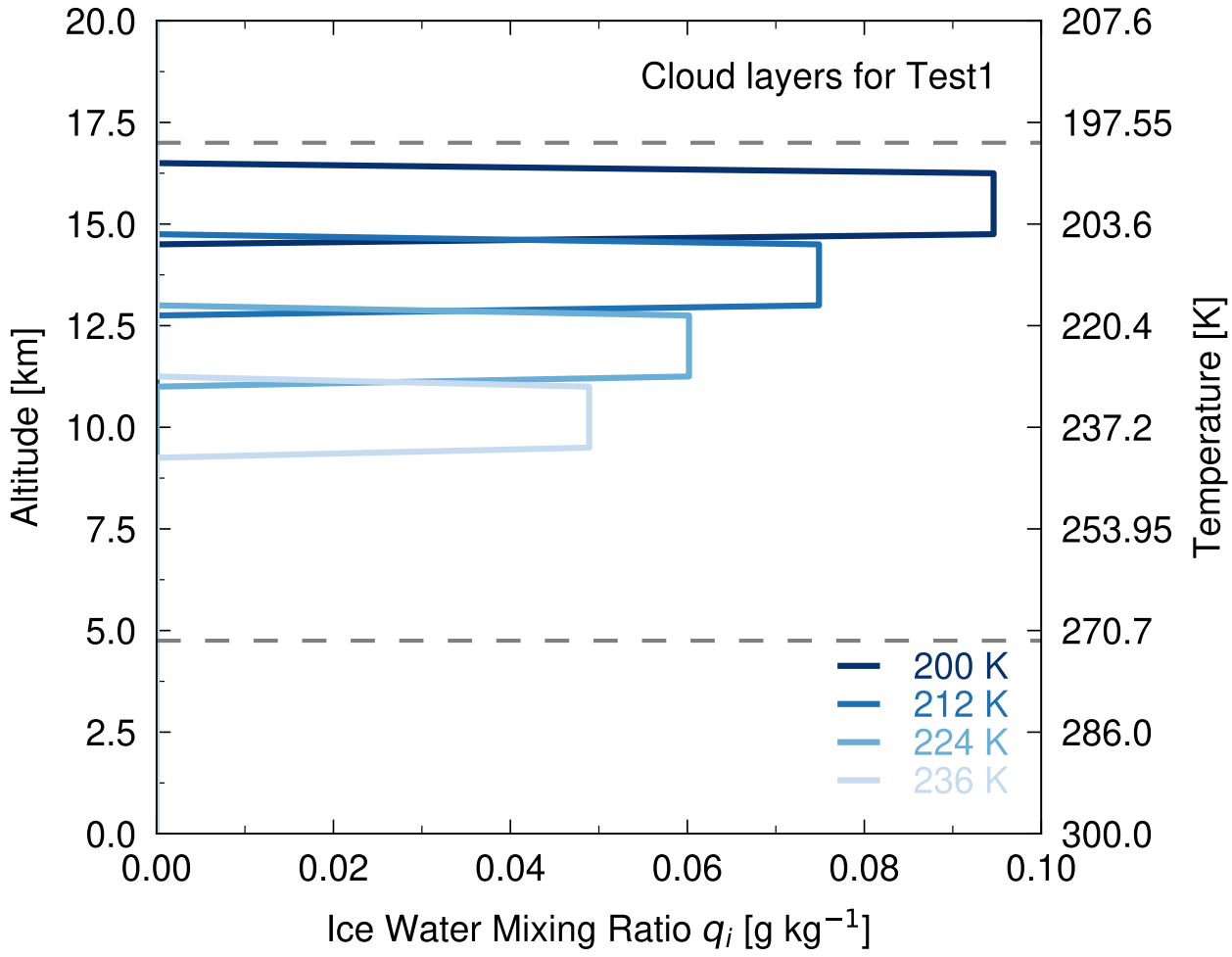

Figure S3. Ice clouds profile for different temperature perturbation levels (Test 1). A geometrical depth of 1.5 km and an IWP of 30 g m^{-2} is used to compute q_i

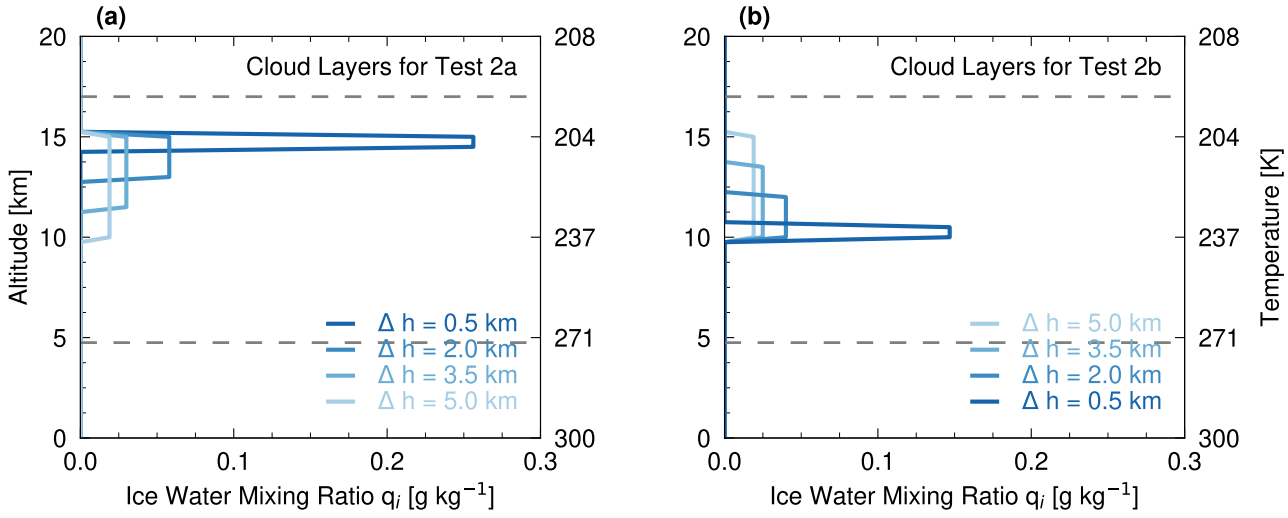

Figure S4. Ice clouds profile for different geometrical depths. Test 2a (a) and test 2b (b). An IWP of 30 g m^{-2} is used to compute q_i.

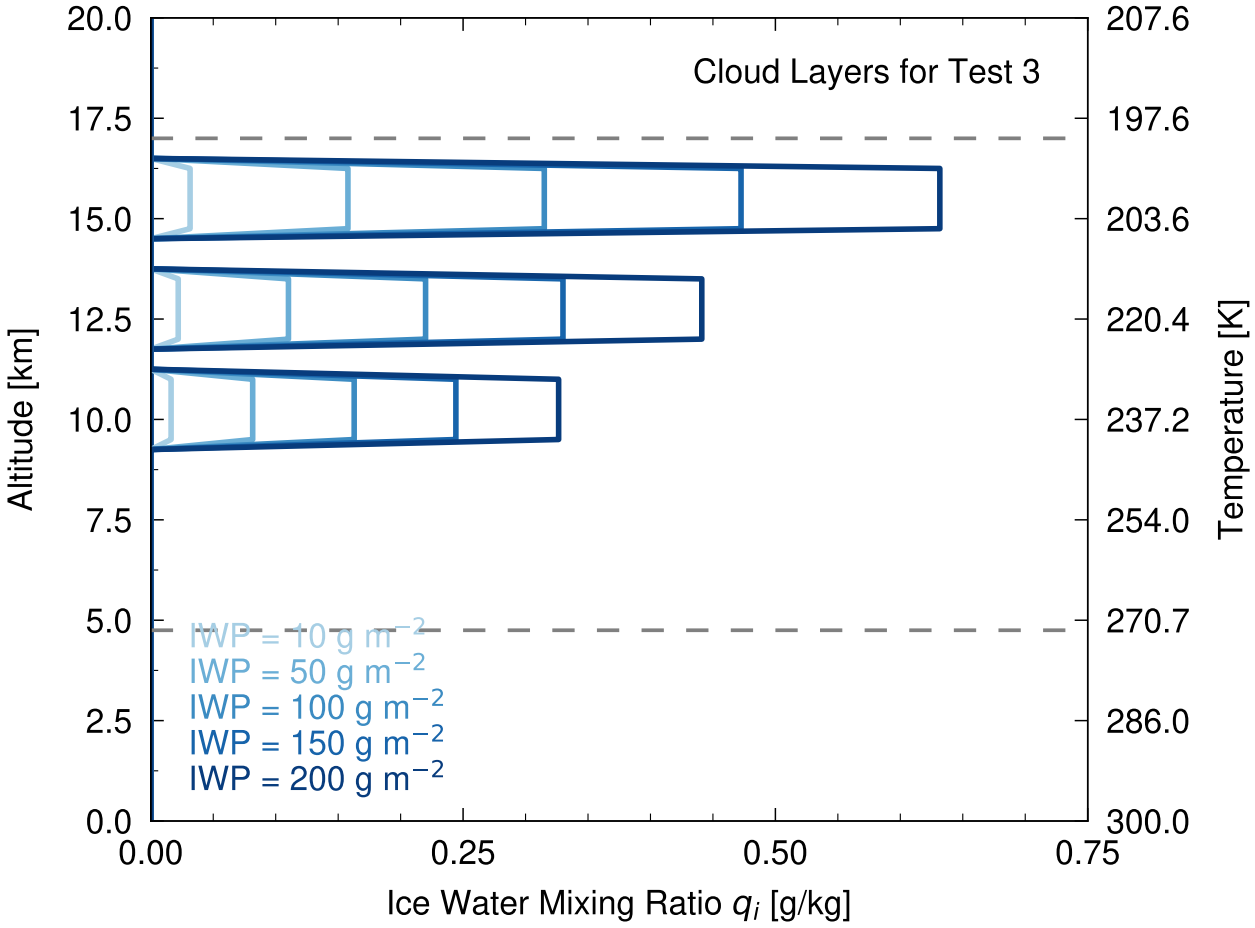

Figure S5. Ice clouds for different IWP and three temperature perturbation levels (Test 3). A geometrical depth of 1.5 km is used to compute q_i

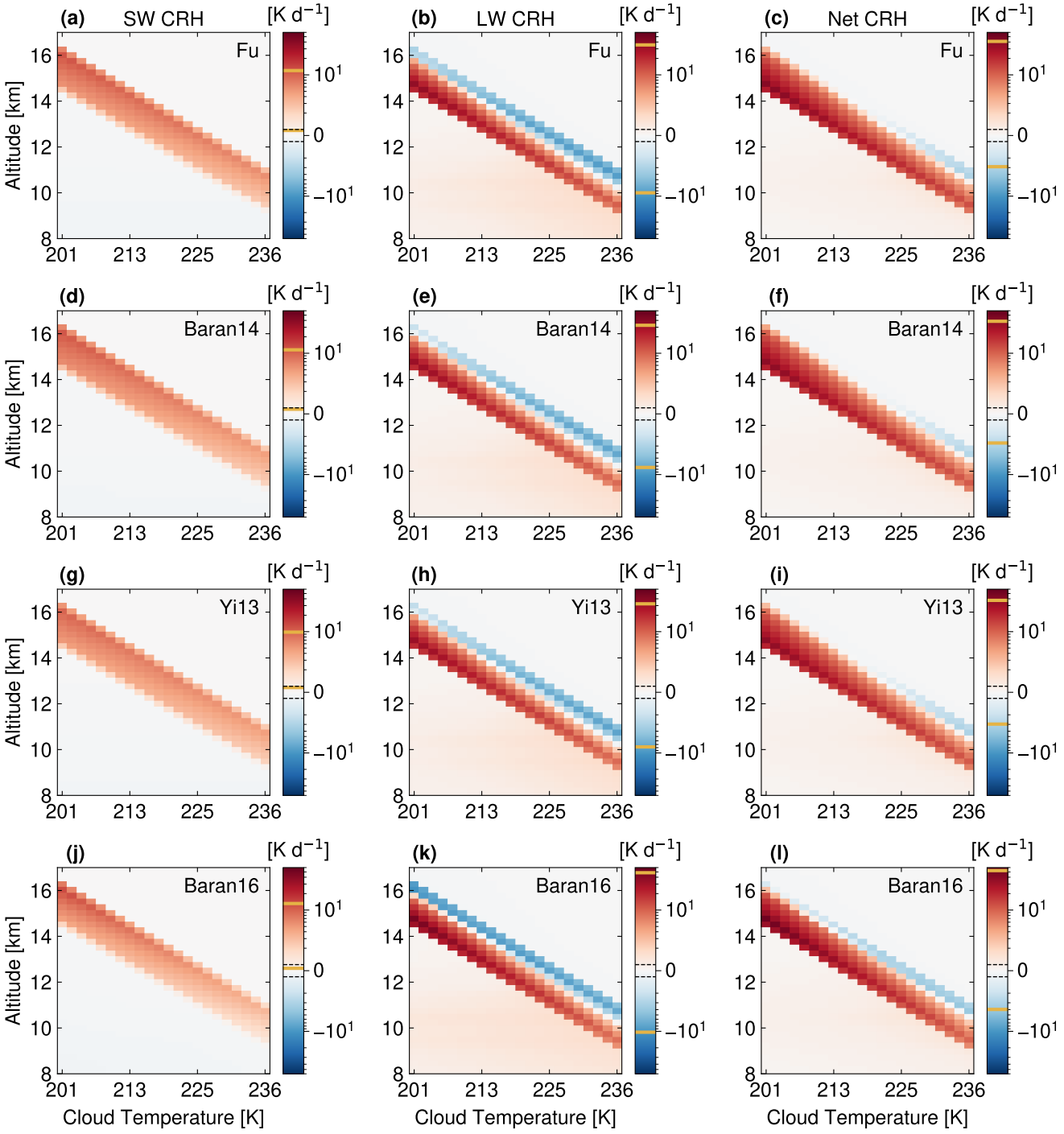

Figure S6. Matrix visualizations including 22 CRH profiles each for middle cloud temperatures from 201 K to 236 K (Test 1). Each column panel shows the corresponding radiative components (SW, LW, and Net), and each row corresponds to the schemes under test. The corresponding height position of the layer cloud is depicted in the y-axis while the CRH magnitude is represented in the color bar, with a general range from -60 to 60 K day^{-1}. Yellow lines in the color bar show the corresponding CRH range for each panel. Black dash lines in the color bar mark the limit between the linear and logarithmic scale in the color bar (1 K day^{-1}).

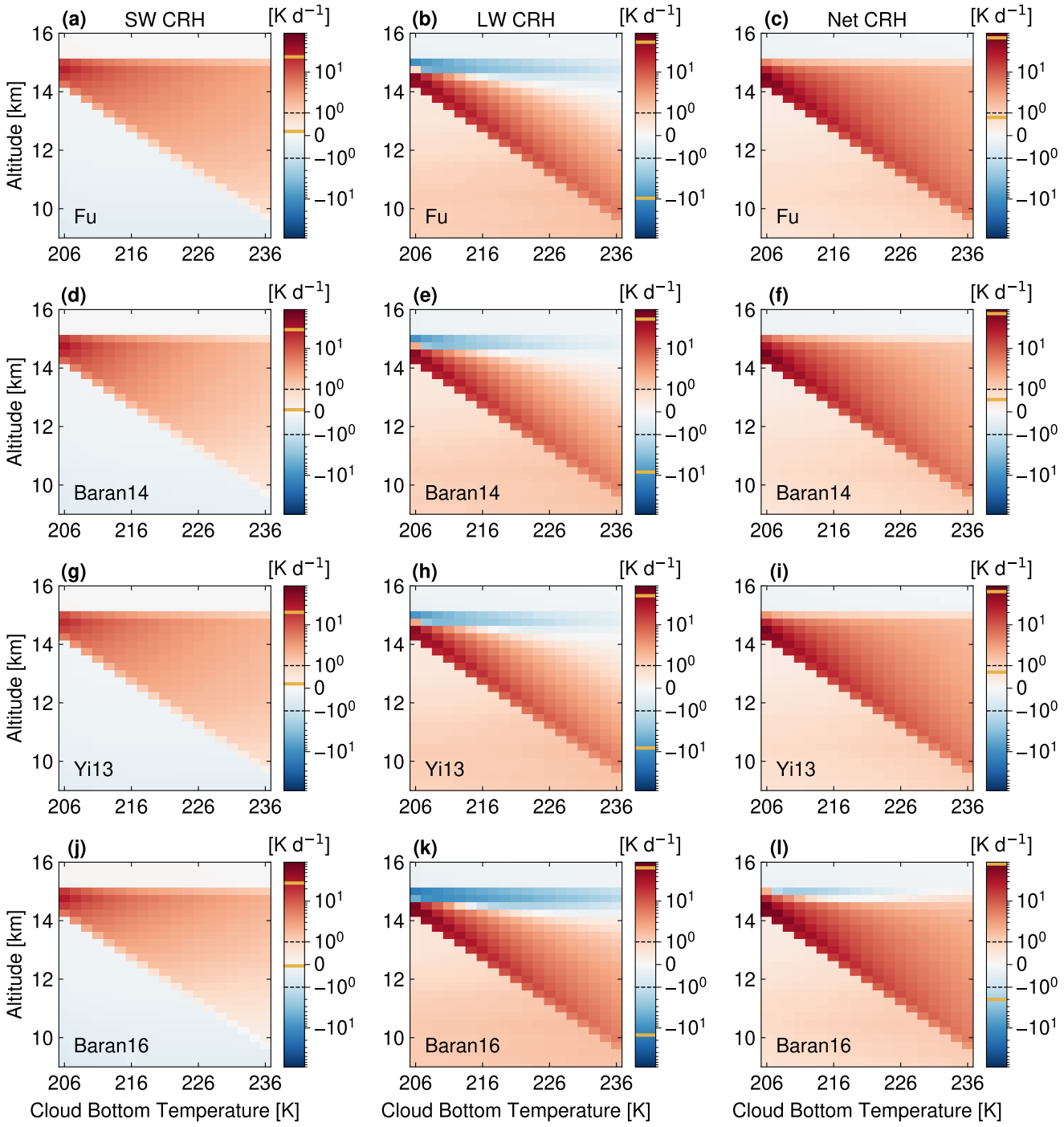

Figure S7. Matrix visualizations including 19 CRH profiles each for cloud depths from 0.5 to 5 km, with fixed cloud top temperature of 203 K (Test 2a). Panels, axes, and colorbar are as in Fig. S6, with a general range from -90 to 90 K day^{-1}.

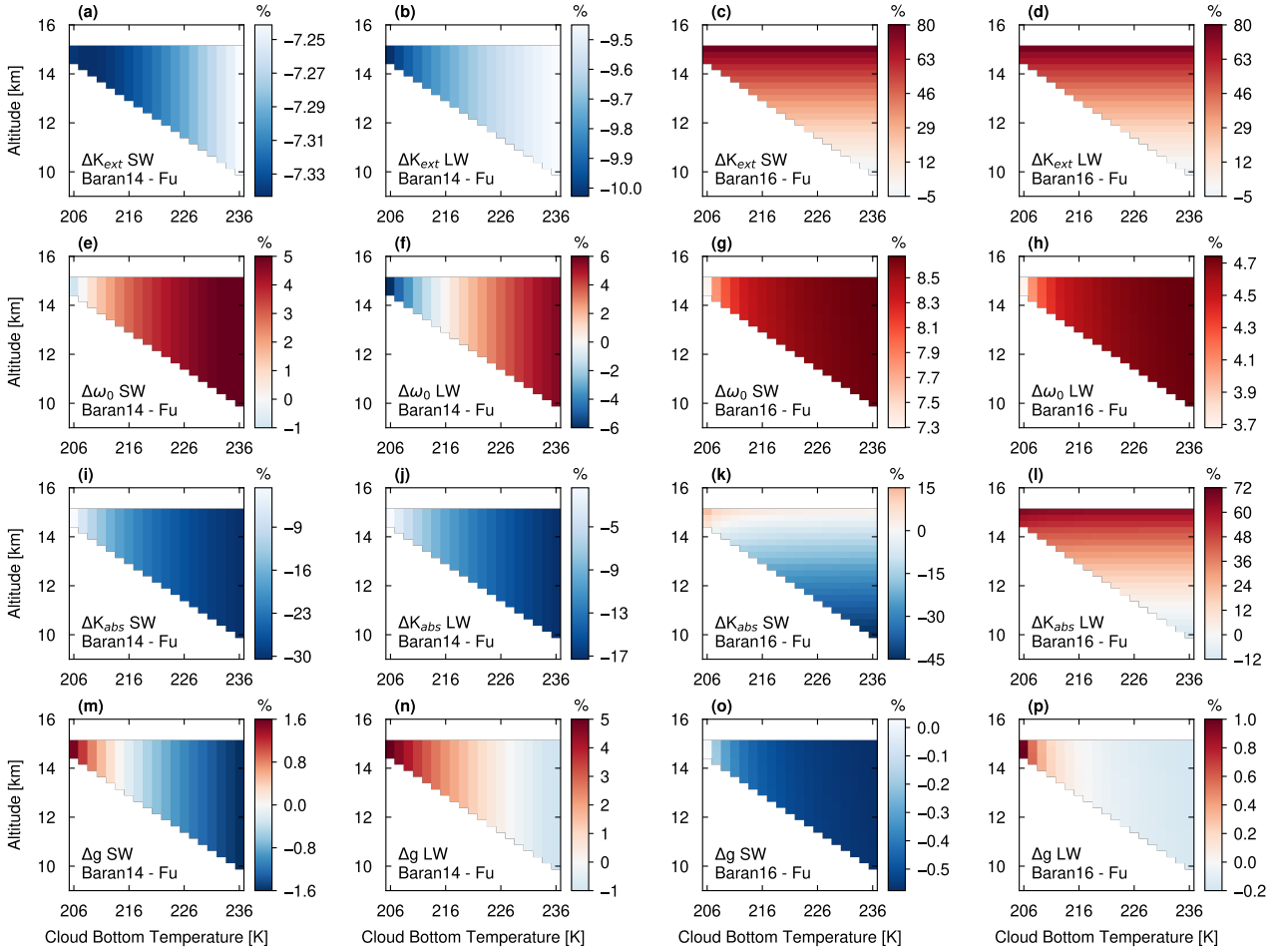

Figure S8. Matrix visualizations including 19 interscheme relative difference profiles for the K_{ext}, ω_0, K_{abs} and g (top to bottom rows), each for cloud depths from 0.5 to 5 km, with fixed cloud top temperature of 203 K (Test 2a). First and second column shows Baran14-Fu interscheme difference for SW and LW components respectively. The same components are shown in the third and fourth column for Baran16-Fu interscheme comparison.

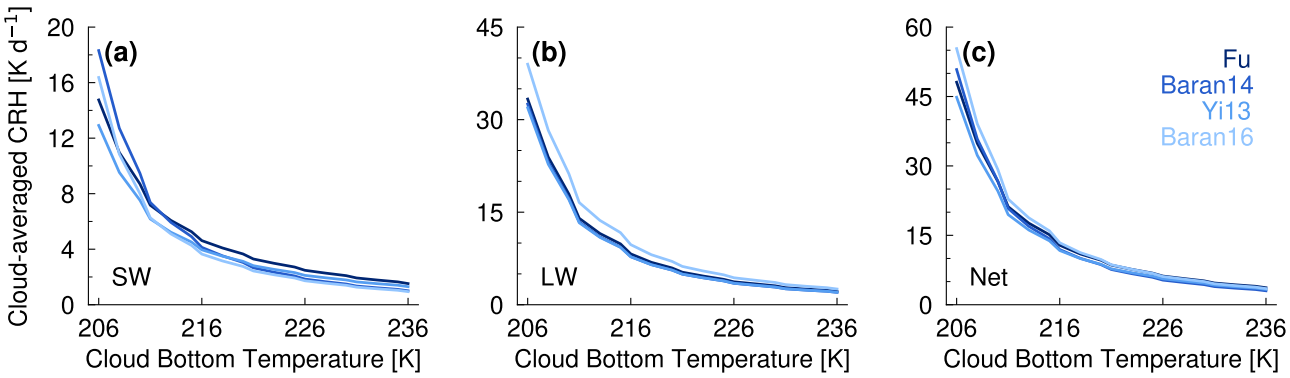

Figure S9. SW (a), LW (b) and Net (c) Cloud-average CRH (y-axis) evaluated for each single-column profile shown in Fig. S7. Cloud bottom temperatures across cloud depths from 0.5 to 5 km, with fixed cloud top temperature of 203 K (Test 2a) are depicted in x-axis. All four ice optical schemes under test are shown from darker blue to light blue, indicating low to high ice complexity level.

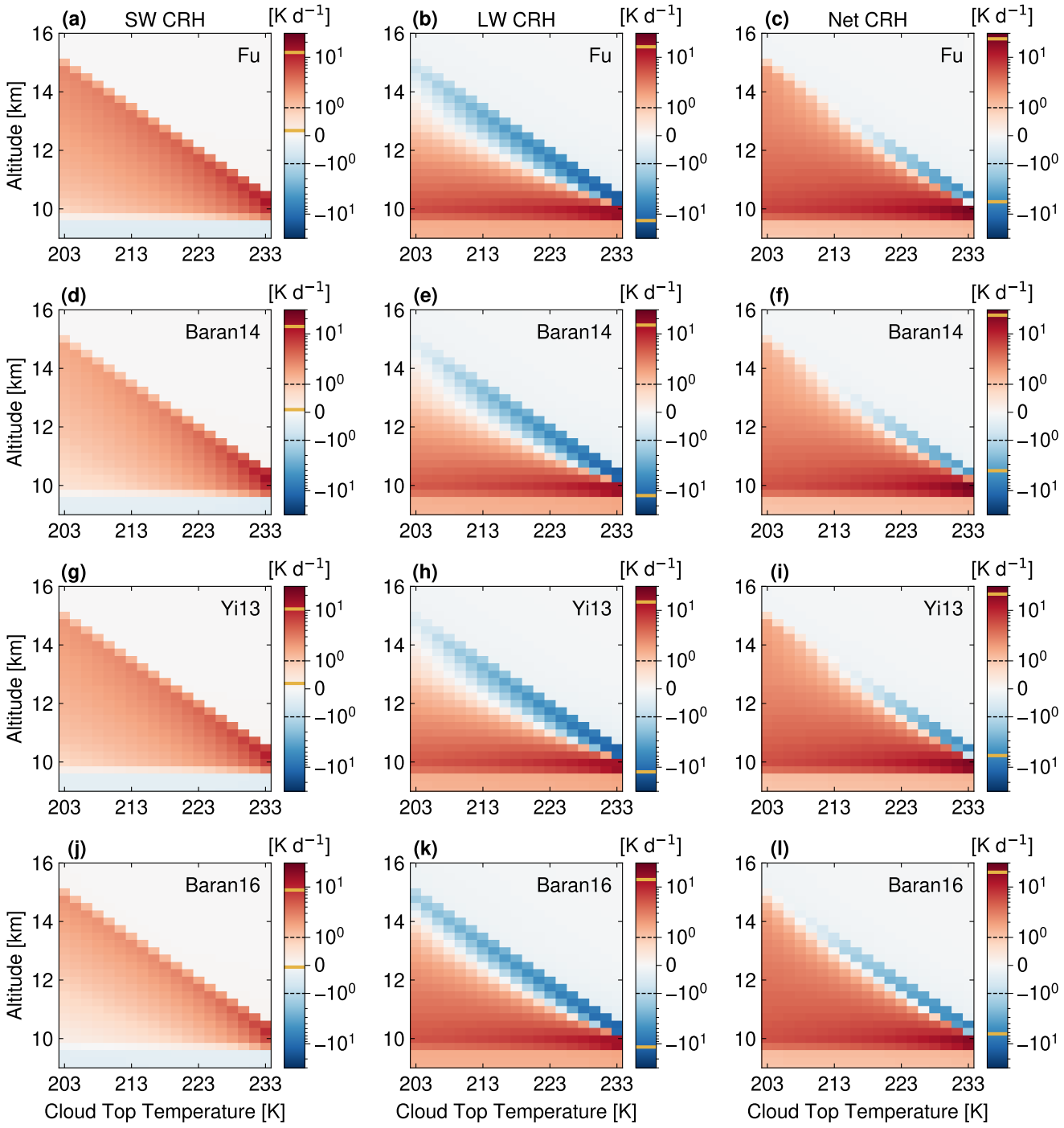

Figure S10. Matrix visualizations with the same depth range as in Fig. S7 and with fixed cloud bottom temperature of 237 K (Test 2b). Panels, axes, and colorbar are as in Fig. S6, with a general range from -30 to 30 K day^{-1}.

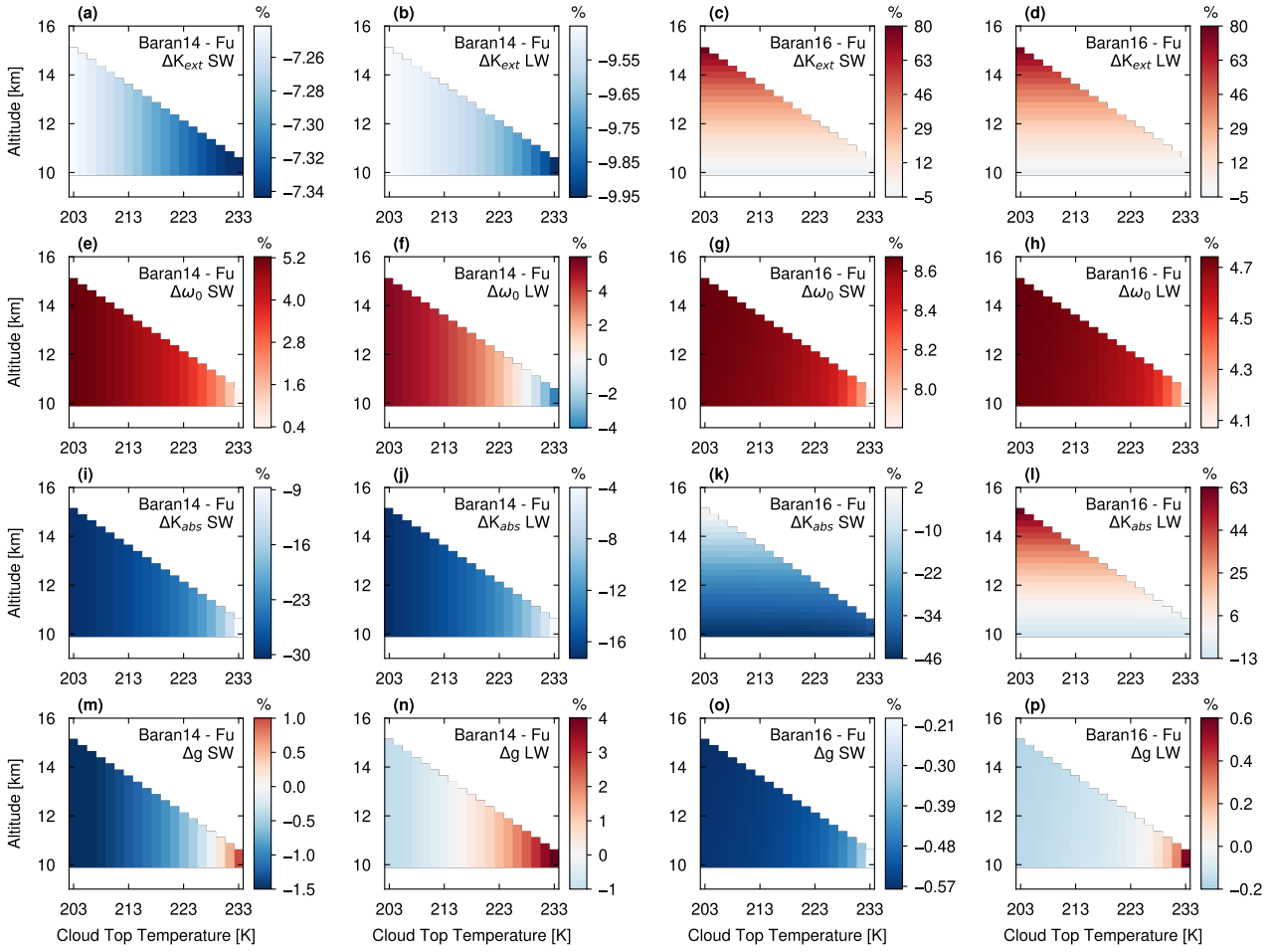

Figure S11. Matrix visualizations including interscheme relative difference profiles for the K_{ext}, ω_0, K_{abs} and g, with the same depth range as in Fig. S10 and with fixed cloud bottom temperature of 237 K (Test 2b). Panels, axes, and colorbar are as in Fig. S8.

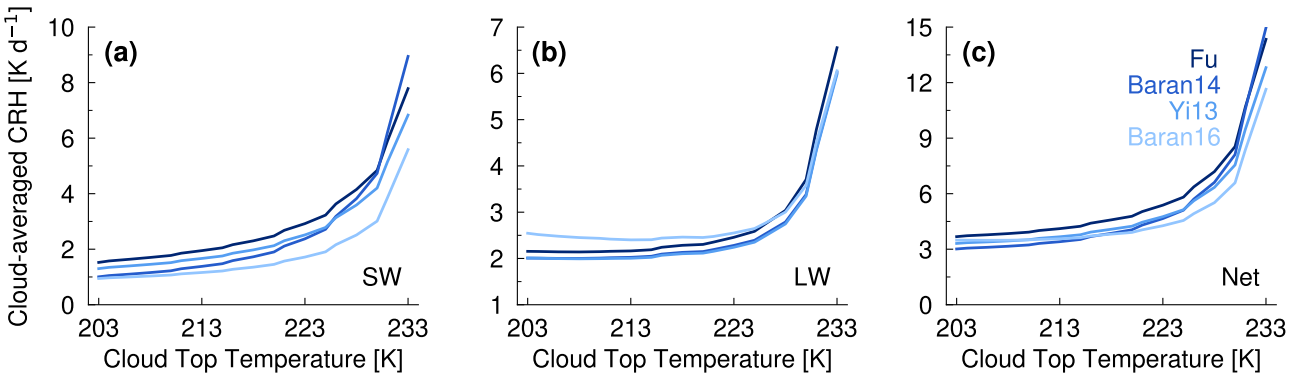

Figure S12. SW (a), LW (b) and Net (c) Cloud-average CRH (y-axis) evaluated for each single-column profile shown in Fig. S9. Cloud top temperatures across cloud depths from 0.5 to 5 km, with fixed cloud bottom temperature of 237 K (Test 2b) are depicted in x-axis. All four ice optical schemes under test are shown from darker blue to light blue, indicating low to high ice complexity level.

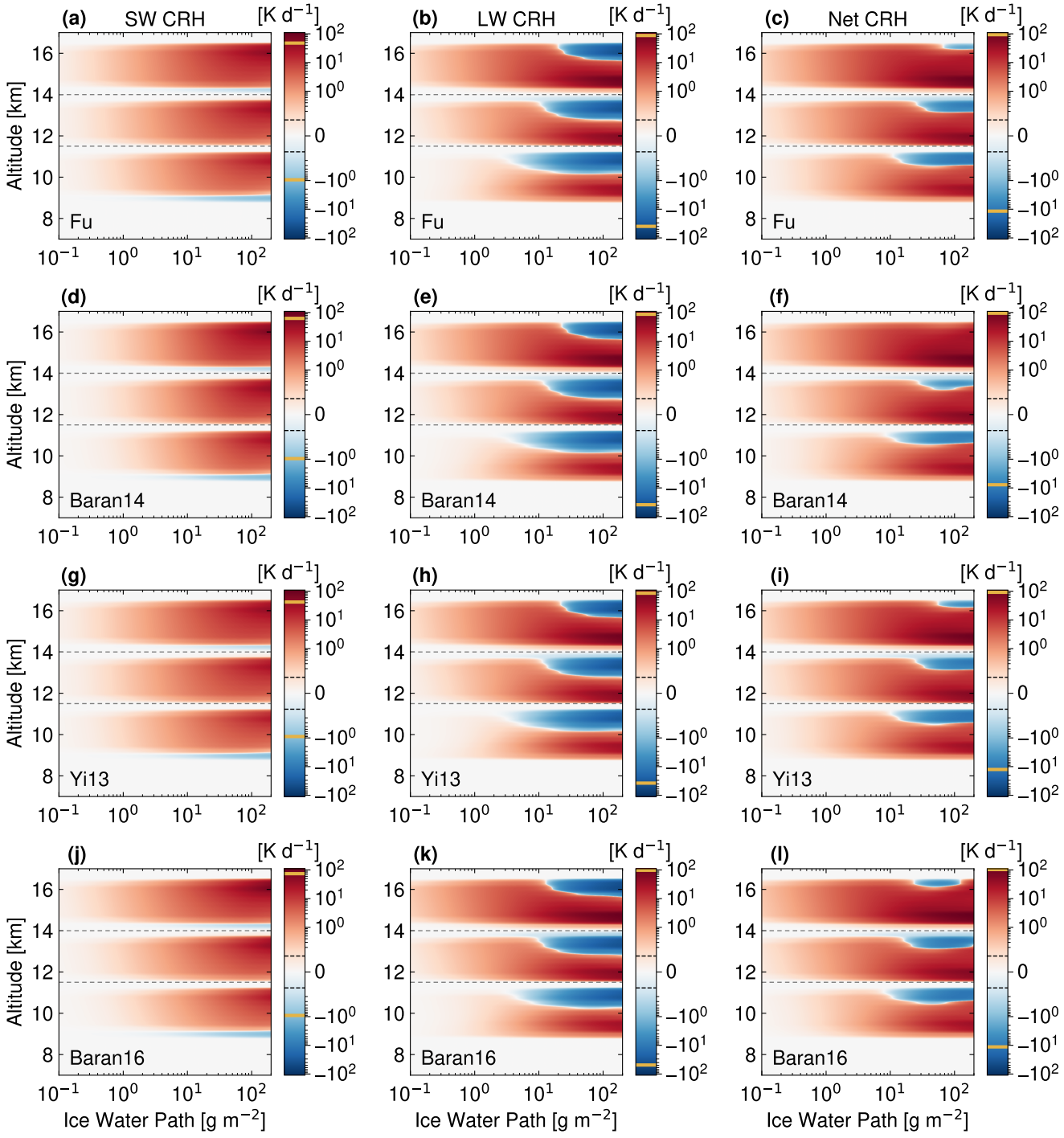

Figure S13. Matrix visualizations including CRH profiles for IWPs from 0.1 to 200 g m^{-2} in Test 3. Three separate differences are shown for cloud temperatures of 201 K, 218 K, and 236 K, corresponding to high, middle, and low altitudes. Panels, axes, and colorbar are as in Fig. S6, with a general range from -100 to 100 K day^{-1}. The limit between the linear and logarithmic scale is 0.01 K day^{-1}.

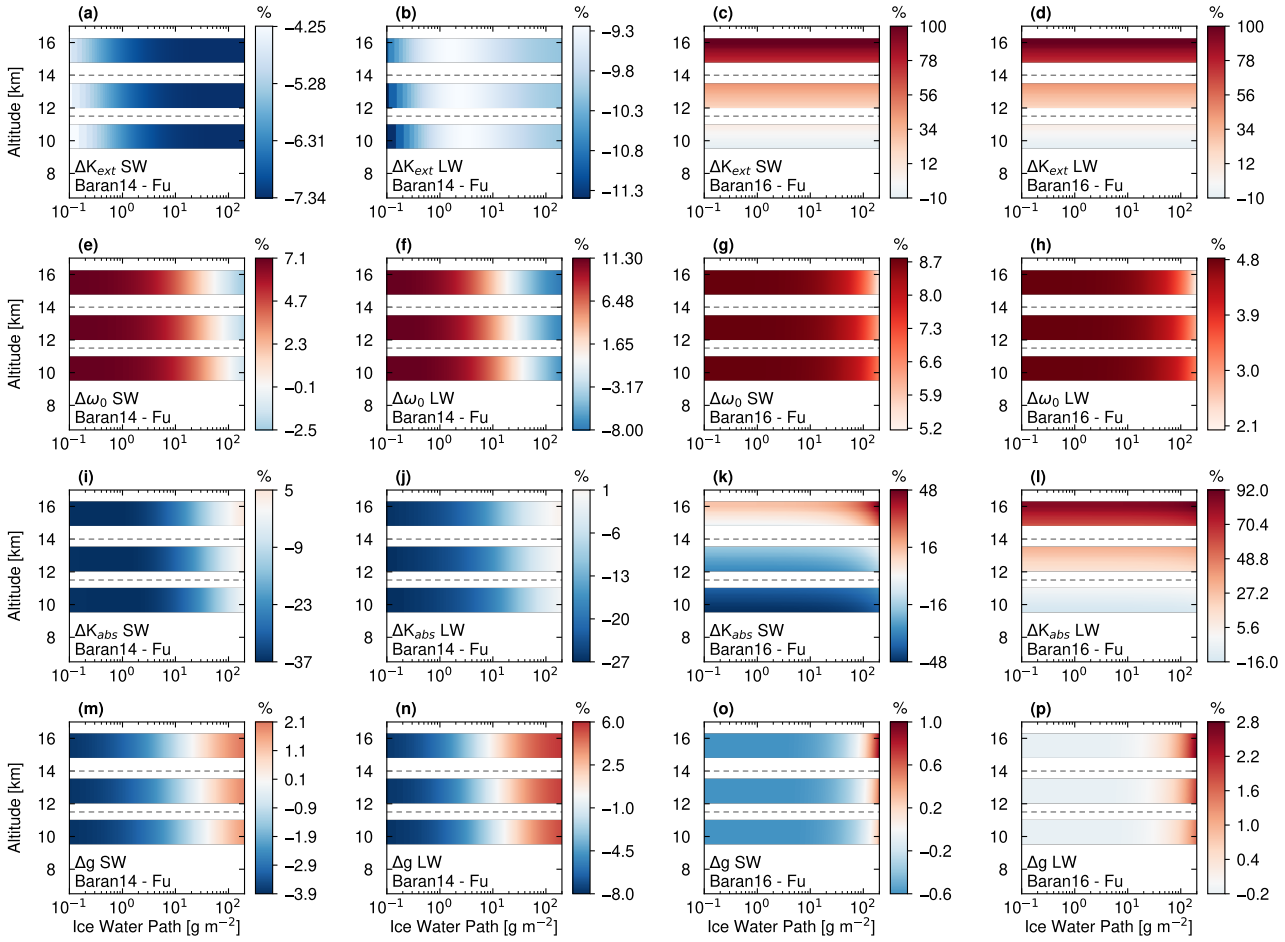

Figure S14. Matrix visualizations including interscheme relative difference profiles for the K_{ext}, ω_0, K_{abs} and g. The IWP range and the three independent cloud layers are as in Fig. S13 (Test 3). Panels, axes, and colorbar are as in Fig. S8.

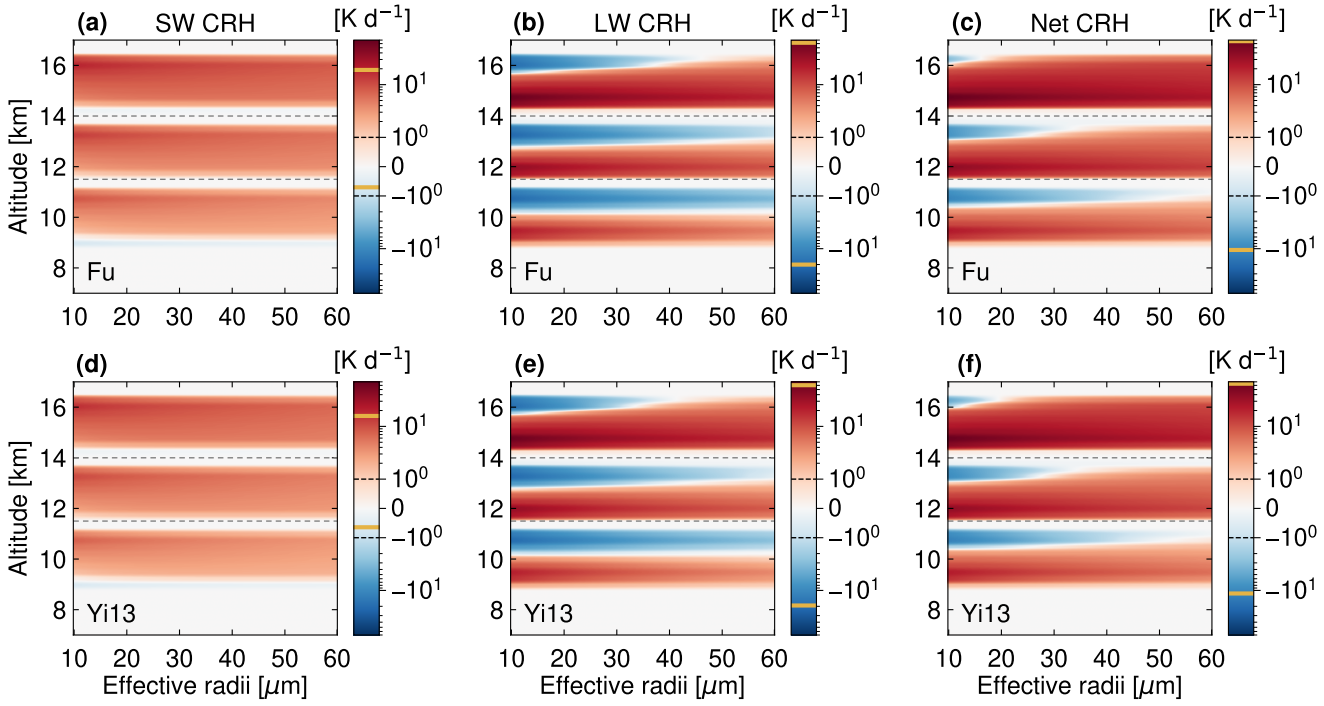

Figure S15. Heating rate matrix visualizations including CRH interscheme difference profiles for ice crystal effective radii ranging from 10 to 60 μm (Test 4). Three separate profiles are calculated for low, middle, and high cloud temperatures of 201 K, 218 K, and 236 K as in test 3. Columns, axes, and colorbar are as in Fig. S6, with a general range from -70 to 70 K day^{-1}. The limit between the linear and logarithmic scale is 1 K day^{-1}.